



Novel Li(Ni_{1/3}Co_{1/3}Mn_{1/3})O₂ cathode morphologies for high power Li-ion batteries

Miodrag Oljaca*, Berislav Blizanac, Aurelien Du Pasquier, Yipeng Sun, Ranko Bontchev, Arek Suszko, Ryan Wall, Kenneth Koehlert

Cabot Corporation, 5401 Venice Ave. NE, Albuquerque, NM 87113, USA



HIGHLIGHTS

- Li(Ni_{1/3}Co_{1/3}Mn_{1/3})O₂ (NCM) materials are produced using Reactive Spray Technology.
- Small particles with substantial intra-particle porosity show improved power rate.
- Synthesis conditions are suitable for large scale manufacturing.

ARTICLE INFO

Article history:

Received 5 July 2013

Received in revised form

7 September 2013

Accepted 24 September 2013

Available online 4 October 2013

Keywords:

Li-ion

Cathode

Spray pyrolysis

Spray conversion

NCM

ABSTRACT

In this paper, we report unique Li(Ni_{1/3}Co_{1/3}Mn_{1/3})O₂ (NCM) materials produced using aerosol based liquid to solid conversion in different reactor configurations and using different atomization methods jointly termed Reactive Spray Technology (RST). A series of experiments was performed at different RST synthesis conditions suitable for large scale manufacturing to produce NCM powders with particle size ranging from 1 to ~10 μm, varying degree of particle porosity and excellent compositional purity. The electrochemical testing in Li-ion cells indicates that NCM materials made via RST have high initial discharge capacity and good first cycle efficiency. NCM materials with small particle size and substantial intra-particle porosity show improved power rate performance at high discharge rates compared to larger particle size NCM. This was attributed to shorter diffusion length in the solid phase, increased electrochemically active surface area and high active phase accessibility due to the combined effect of smaller particle size and internal porosity. Specific capacity of small-particle NCM made by RST method was 167 mAh g⁻¹ at 0.2 C and 137 mAh g⁻¹ at 10 C, which compares favorably to 160 mAh g⁻¹ at 0.2 C and 97 mAh g⁻¹ at 10 C for NCM made by co-precipitation method having 10 μm average particle diameter.

© 2013 Elsevier B.V. All rights reserved.

1. Introduction

Rechargeable lithium-ion batteries (LIB) have been the main power source for a wide range of electronic consumer products since their initial commercialization in the early 1990s. At present, they are being extensively evaluated for large-scale applications, such as hybrid electric vehicles, plug-in hybrid electric vehicles and all-electric vehicles, to reduce dependence on oil and alleviate air pollution. For such applications, LIB technology requires long-lasting batteries with high power and high energy density [1,2].

Cathode is a major performance limiting material in LIB technology. Current generation of LIB cathode materials are mainly multi-component mixed-metal oxides or phosphates. These materials are produced commercially by either solid state or co-precipitation processes. Compositional homogeneity and high purity are inherently difficult to achieve in solid state routes. Li(Ni_{1/3}Co_{1/3}Mn_{1/3})O₂ (NCM) is one of the most promising cathode materials for applications in Li-ion batteries [3,4] and it is currently made using co-precipitation and calcination process [5,6]. In this process, NiCoMn(OH) precursors are produced using precipitation followed by lithiation and heat treatment of that precursor at high temperatures in a secondary step. While co-precipitation process can deliver better homogeneity than solid state process, it involves many unit operations including precipitation, filtration, drying, and calcination which dramatically increase complexity of

* Corresponding author.

E-mail address: miki.oljaca@cabotcorp.com (M. Oljaca).

manufacturing process. In addition, it is difficult to effectively remove sodium and sulfur impurity, which is introduced in precipitation step during filtration. While precipitation processes can produce particles with various morphologies it is often difficult and costly to produce very small particles with controlled porosity. Current commercial NCM materials typically come in size range from 5 to 15 μm with various ratios of main elements and different surface properties [7–10].

In attempts to overcome some of the disadvantages of precipitation and solid-state synthesis routes, several new methods, such as sol–gel [11], ultrasonic spray pyrolysis [12], solution spray drying [13], have been developed and applied to produce $\text{Li}[\text{Ni}_{1/3}\text{Co}_{1/3}\text{Mn}_{1/3}]_{\text{O}_2}$ [14]. These methods are capable of producing homogeneous materials with controllable particle size [15] but these routes are typically based on complex precursors, laboratory scale atomization techniques and expensive energy sources which may not be suitable for cost-effective large scale production of cathode materials.

Spray pyrolysis [16] is an attractive method for mass production of ultrafine powders due to speed of reaction, control of composition, and control of particle size [17]. The method has found application for the production of Li-ion cathode powders: layered $[\text{Ni}_{1/3} + x\text{Co}_{1/3}\text{Mn}_{1/3} - 2x\text{Mo}_x]\text{O}_2$ cathode materials have been prepared by ultrasonic spray pyrolysis [18], $\text{LiNi}_{0.8}\text{Co}_{0.2}\text{O}_2$ has been prepared by a spray-drying method [19], ultrafine LiCoO_2 powder was prepared by a spray-drying method [20], LiMn_2O_4 cathode materials were made by flame-assisted spray technology [21]. LiFePO_4 has also been synthesized by highly-flexible and scalable flame spray pyrolysis [22]. Kang et al. have described the preparation of $\text{Li}_{x}(\text{Mn}_y\text{Ni}_{1-y})\text{O}_z$ cathode powders by spray pyrolysis [23], as well as fine-sized $\text{LiNi}_{0.8}\text{Co}_{0.15}\text{Mn}_{0.05}\text{O}_2$ cathode particles by spray pyrolysis from polymeric precursor solutions [14].

In contrast to most of the previously published work, the present cathode materials were prepared on pilot size units capable of producing larger quantities of materials and scalable to tens of kg per hour, where atomization techniques can be either ultrasonic or non-ultrasonic spray nozzles, and heat sources are either inline electric furnaces or propane gas [24]. Combination of different atomization methods and reactor configurations based on liquid to solid conversion is jointly termed here as Reactive Spray Technology (RST). The RST synthesis enables production of cathode particles from sub-micron size up to over ten microns diameter.

Initial rough engineering estimate indicate that RST platform at scale could economically compare favorably to co-precipitation synthetic route. Preliminary work shows that the difference in cost between nitrate and sulfate precursors (raw materials for both RST and co-precipitation) is negligible when compared on a metal basis. This is reasonable as salts are prepared by dissolving oxide, hydroxide or carbonate in sulfuric or nitric acid. However, the difference in operating cost for the two precursors can be significant. In co-precipitation, the anions are left in the waste water stream and must be addressed there based on local waste water discharge limits. In RST, the anions decompose at high temperature generating NO_x or SO_x and other byproducts that must be abated in the gas phase. At large scale it could be possible to recover nitric or sulfuric acid from the offgas in RST. Nitric or sulfuric acid could be concentrated and used to produce precursor salts by dissolution of metal oxides, hydroxides or carbonates. RST technology could also have favorable direct labor cost. The co-precipitation route is mainly a batch operation with large number of process steps. RST is potentially a continuous, largely automated process with low direct labor requirements. Initial rough estimate suggests that RST could favorably compare to co-precipitation in terms of capital and operating costs due to the different scalability of two technologies. At very large scale ($>2000 \text{ MT year}^{-1}$) it becomes increasingly hard

to obtain desired mixing rates in the stirred tank reactor (co-precipitation method) and further scale would then require replication – more expensive to purchase and operate. RST typically can be scaled to a greater capacity before replication is required.

Flexibility of RST process in producing variety of compositions (layered, spinel, olivine), including additional doping in a single process step by simple control of the precursors stoichiometric composition, using the same equipment and reactor configuration, has potential to add further to the economic appeal of RST process. Further optimization aimed at introducing surface coating downstream in the reactor and control over temperature and residence time to eliminate subsequent calcination step could result in final economy of scale well aligned with targets in cost sensitive applications such as vehicles electrification.

In a typical co-precipitation process, the synthesis step is followed by multiple washing, lithiation and extended calcination at elevated temperature. The RST process has potential to improve compositional uniformity of the product and significantly reduce energy cost of NCM production. In RST process, all precursors including Li are pre-mixed at the molecular level prior to introduction into the RST reactor. This enables excellent control of compositional homogeneity to a degree that is hard to achieve with co-precipitation especially at large scale production. The energy cost of extended calcination (sometimes $>24 \text{ h}$) at high temperatures ($\sim 1000^\circ\text{C}$) is significant. Furthermore, it is often necessary to utilize expensive calcination equipment because of the calcination conditions. The RST enables either a complete elimination of the calcination step or significant reduction in calcination time and temperature. For example, in this paper we demonstrate that RST can be used to produce NCM with only 2 h of calcination at 800–900 $^\circ\text{C}$. The energy cost and process simplification are significant potential benefits of RST when considering large scale production for Li-ion industry.

In this paper, $\text{Li}(\text{Ni}_{1/3}\text{Co}_{1/3}\text{Mn}_{1/3})\text{O}_2$ powders were synthesized by reactive spray technology from a solution feedstock containing Li, Ni, Co and Mn precursors which ensures excellent control of compositional homogeneity. Various atomization techniques and reactor designs were explored in order to identify design parameters that will not only produce desired particle properties but also enable cost effective large scale production. $\text{Li}(\text{Ni}_{1/3}\text{Co}_{1/3}\text{Mn}_{1/3})\text{O}_2$ powders with particle size ranging from <1 to $>10 \mu\text{m}$ and various degree of porosity were produced and characterized. The electrochemical performance of $\text{Li}(\text{Ni}_{1/3}\text{Co}_{1/3}\text{Mn}_{1/3})\text{O}_2$ cathodes were studied in half-cell configuration for initial capacity, discharge rate capability and cycle-life under accelerated conditions of 60 $^\circ\text{C}$.

2. Experimental

2.1. Materials synthesis

$\text{Li}(\text{Ni}_{1/3}\text{Co}_{1/3}\text{Mn}_{1/3})\text{O}_2$ (NCM) powders were prepared by Reactive Spray Technology which combines both liquid phase and solid state processing (Fig. 1). The major attributes of this approach are the flexibility to achieve unique compositions and microstructures while allowing for high volume manufacturing with low cost. The processing starts with the formulation of a liquid feedstock that contains either dissolved or suspended reagents which act as precursors to the final product or as supports. The liquid, together with a gas, is then fed to an atomization unit where the liquid is converted into an aerosol. The gas stream containing the aerosol is then heated in a gas phase processing unit to effect the physical and chemical conversion of the droplets to the final powder. The final product is separated from the gas stream using conventional powder collection methods leaving only a gaseous effluent (no liquid effluent to be disposed). The final powder microstructure and

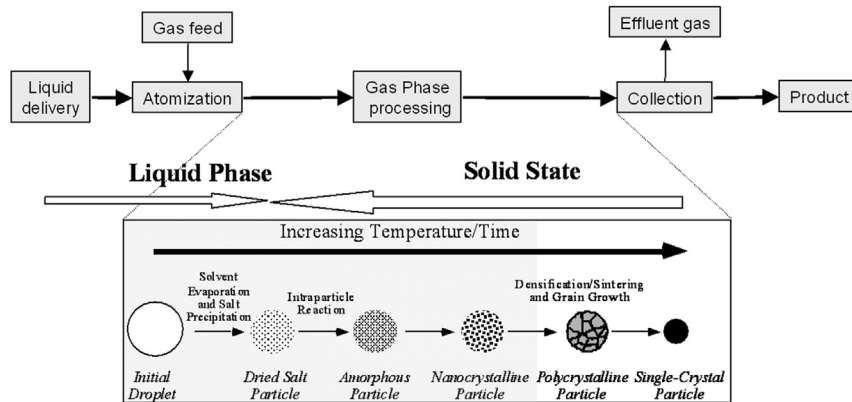


Fig. 1. Schematic representation of spray-based particle manufacturing process.

composition depend on the residence time, temperature, the reactive nature of droplet components and the composition of the gas. The physical and/or chemical evolution of the particles can be arrested at any stage by quenching of the reaction media. Therefore this process can be used to produce a wide variety of materials compositions combined with unique microstructures and morphologies.

In this paper, $\text{Li}(\text{Ni}_{1/3}\text{Co}_{1/3}\text{Mn}_{1/3})\text{O}_2$ (NCM) powders were prepared from an aqueous solution of $\text{Ni}(\text{NO}_3)_2 \cdot 6\text{H}_2\text{O}$ (Aldrich), $\text{Co}(\text{NO}_3)_2 \cdot 6\text{H}_2\text{O}$ (Aldrich), $\text{Mn}(\text{NO}_3)_2 \cdot 4\text{H}_2\text{O}$ (Aldrich), and LiNO_3 (Aldrich). The solution was then atomized by using either a 1.65 MHz submerged ultrasonic spray generator or proprietary air-assist nozzles to produce droplets that were carried by a carrier gas into a high-temperature reactor that can be heated internally or externally. The reactor temperature was varied from 600 °C to over 1500 °C by controlling reactor input energy and design. The residence times in the reactor zone varied from <100 ms to ~10 s. The overall solution solids loading of the nickel, cobalt, manganese and lithium components was 5 wt %. The as-produced NCM powders were alternatively post-treated at a temperature of 900 °C for 4 h under air atmosphere.

Physical properties and electrochemical performance of materials made by RST were compared to NCM powder made by conventional co-precipitation method. Physical characteristics of co-precipitation made powders can be found in tables in the manuscript. Based on the physical characterization and electrochemical performance, NCM made by co-precipitation method used in this study has similar characteristics and performance published for different commercial NCM grades.

2.2. Analytical methods and characterization

The crystal structure of the synthesized powders was carried out using X-ray diffractometry (XRD, Bruker D-8 Advance instrument) using Ni-filtered $\text{Cu-K}\alpha$ radiation at 40 kV/40 mA, within 10–90° 2-theta range. The analysis was performed using the TOPAS software and Rietveld's structure refinement method.

Powder morphology was studied using scanning electron microscopy (Hitachi S-5200 field emission SEM), generally operated at an accelerating voltage of 2.0 kV, coupled with a PGT EDS system and PGT Spirit software for elemental mapping and EDS.

The BET surface area and porosity of each sample was measured by multi-point Nitrogen adsorption/desorption cycles in a Micromeritics Tristar 3000 apparatus. Each sample was first degassed in vacuum at 200 °C for 2 h and ultra-high purity N_2 gas was used in the measurement.

Particle size distribution analyses were performed on BlueWave particle size analyzer. 0.20 g sample is mixed with 50 ml D.I. water and 3 drops of Darvan C surfactant. The resulting solution is sonified for 3 min with Branson 450 before loading.

2.2.1. Electrochemical methods and characterization

All cathode powders were coated on 17 microns thick Al foils using PVDF Solef 1030 as binder, carbon black and graphite conductive additives. The electrode slurries were dispersed in NMP using a SPEX mill with two zirconia media for 30 min. The electrodes were dried at 80 °C for ~15 min, then at least 4 h at 100 °C under vacuum prior to coin-cell assembly in Ar filled glove-box (MBraun). A constant mass loading of 9 mg cm^{-2} corresponding to a capacity loading of $\sim 1.5 \text{ mAh cm}^{-2}$ was used for all the electrochemical measurement reported herein. Electrodes were calendared to a thickness of ~40 microns resulting in porosity of 15–20%. 15 mm calendared cathode discs where tested in 2032 coin-cells (Hosen) versus lithium anode. Whatman GF/D fiberglass separator and EC–DMC–EMC (1:1:1) with 1% VC, 1 M LiPF_6 electrolyte (Novolyte, <20 ppm water) were used.

The initial charge/discharge capacities of the samples were measured through cycling in the 2.8–4.3 V potential range at a constant current density of 0.2 C. Capacity versus current curves were generated with constant current charging of 0.5 C then constant voltage of 4.3 V with current cutoff of 0.02 C, and discharge rates of 0.2 C, 0.5 C, 1 C, 2 C, 5 C and in some cases 10 C, 15 C, 20 C. The cycle performances of the cathode powders at an elevated temperature of 60 °C were measured at a constant current density of 0.5 C. Electrochemical impedance measurements were performed on the coin-cells with an EG&G 2273 using PowerSine software, in the 1 MHz–10 mHz range and 10 mV signal amplitude.

3. Results and discussion

3.1. Materials synthesis and physical characterization

Fig. 2 shows XRD patterns for NCM powder prepared by RST at different reactor temperatures using ultrasonic aerosol generation and in-line electrical heat source. For NCM powders made at lower reactor temperature (450 °C) decomposition of nitrate precursors was incomplete and significant amount of precursors remained undecomposed, as witnessed by TGA analysis (not shown). Powders were also only partially converted into the right crystal phase, and resembled more a rock-salt phase instead of the NCM crystal layered phase. For samples made at higher reactor temperatures, the XRD analysis and Rietveld refinement indicates pure $\text{Li}[\text{Ni}_{1/3}\text{Co}_{1/3}\text{Mn}_{1/3}]$

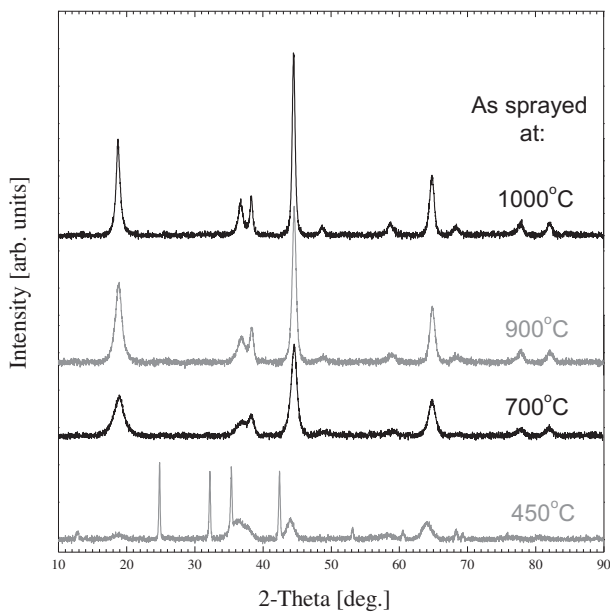


Fig. 2. XRD pattern of NCM powders obtained by Reactive Spray Technology at various reactor temperatures.

$\text{Co}_{1/3}\text{Mn}_{1/3}\text{O}_2$ phase with no peaks from individual oxides. Based on the Rietveld analysis, NCM materials made by RST belongs to the R-3m space group with lattice parameters $a = 2.863 \text{ \AA}$, $c = 14.234 \text{ \AA}$ and average grain size (from XRD) ranging from 8 nm, for as sprayed material made at 750°C reactor temperature, to 265 nm for same powders calcined at 900°C for 24 h.

After RST step all powders have morphology consisting of porous spherical particles formed by agglomeration of smaller particulate aggregates 20–50 nm in size. The particle size during the RST processing can be controlled by solution concentration, droplet size and other process parameters. Each droplet will become a particle and simple correlation between process conditions and final particle size distribution can be established. Results of physical characterization of as-sprayed materials (after RST step) are provided in Table 1.

With the exception of the material made at the lowest reactor temperature, which contains significant amount of un-decomposed precursors, other samples show the trend in reduction of the surface area with increasing the reactor temperature. Surface area, in the entire reactor temperature range, is between 20 and $70 \text{ m}^2 \text{ g}^{-1}$, and spherical particles show significant amount of internal porosity as showed in Table 1 by the total pore volume from single point N_2 BET adsorption measurements. Particle size also decreases with the increase in reactor temperature. All samples have D_{50} of less than

$2 \mu\text{m}$, much smaller than $\sim 5 \mu\text{m}$ which is typical lower limit of the co-precipitation process. Since the conditions of the ultrasonic aerosol generation was the same for all samples, initial droplet size and droplet size distribution is similar. Consequently, higher temperature results in increased particle densification (as schematically shown in Fig. 1) and reduction in both particle size and internal porosity as shown in Table 1.

Crystal size of the final NCM powder is one of the critical properties directly affecting reversible Lithium insertion/deinsertion capacity in Li-ion battery cathodes. Correlation between the primary crystal size and the reversible Lithium capacity at 0.2 C rate is shown in Fig. 3(b). It was found that 0.2 C electrochemical capacity of the NCM powders increases with crystal size, up to a value of $\sim 165 \text{ mAh g}^{-1}$ for crystal size of $\sim 200 \text{ nm}$, but no further improvement was observed at larger crystal size. Optimal size of the primary crystals therefore is in the range 180–220 nm for which the reversible capacity is maximized at $\sim 165 \text{ mAh g}^{-1}$.

The crystallinity of NCM powders can be improved by increasing the reactor temperature and residence time, potentially opening possibility for one step continuous manufacturing process utilizing Reactive Spray Technology. In this study, we mostly explored post treatment at different temperatures and treatment times to achieve desirable size of the primary crystals. One of the general attributes of RST process, applicable also to NCM type materials made in this study, is intimate and homogenous precursor mixing (including Lithium) at the atomic level. The elemental components are in close proximity to one another thus not requiring long heat treatment steps to overcome slow solid state diffusion. This feature of materials made using RST is expected to result in shortening of the heat treatment step in cases where thermal post-treatment is needed. Moreover, the optional post treatment step can typically be performed at much lower temperatures due to the element mixing at the atomic level and short diffusion paths. Effect of calcination time and the calcination temperature on the size of the primary crystals is shown in Fig. 3(a). SEM images in Fig. 4 show that particle size and morphology remain largely unchanged after optional post-treatment step which opens possibilities for some unique powder morphologies. Higher magnification SEM images reveal that smaller aggregates within the particle are more crystalline after the post-treatment step.

When calcination is conducted at 900°C desirable crystal size is achieved after only 2 h, therefore confirming benefit of RST in significant reduction of post-treatment time. Implications are significant-combination of high throughput RST process with short thermal post-treatment have potential for significant materials cost reduction through increased throughput of such commercial process.

Fig. 5 shows XRD pattern for NCM powder produced by RST at 700°C and post-treated at 900°C for 2 h in air. In the same figure XRD pattern of 700°C as-sprayed powder is also provided. It is important to note that the right crystal phase has been achieved already after the RST step. Post-treatment therefore results only in improvement in crystallinity through the primary crystal growth. No crystalline impurities of any kind have been detected after post-treatment. The Co: Mn: Ni ratio was virtually 1 with coefficients differences of ± 0.01 .

Basic physical properties of material sprayed at 700°C reactor temperature before and after post-treatment at 900°C for 4 h in Air are shown in Table 2. For comparison, properties of NCM powder made by co-precipitation method are also provided.

Surface area of as sprayed material ($72.7 \text{ m}^2 \text{ g}^{-1}$) reduced to $2.05 \text{ m}^2 \text{ g}^{-1}$ after calcination at 900°C in air for 4 h. Particle size increased somewhat, but the morphology overall remained very similar to the morphology of the starting as-sprayed powder. As we have already shown (Fig. 3(a)), calcination at high temperature

Table 1
Physical properties of as-sprayed materials at different reactor temperature.

RST temperature	N_2 BET SA ($\text{m}^2 \text{ g}^{-1}$)	Pore volume from single point N_2 BET adsorption ($\text{cm}^3 \text{ g}^{-1}$)	D_{mean} volume (microns)	D_{10} (microns)	D_{50} (microns)	D_{90} (microns)
450 °C	23.5	0.054	1.704	0.585	1.293	3.364
700 °C	72.7	0.191	1.518	0.482	1.240	2.904
900 °C	31.8	0.141	1.444	0.322	1.174	2.884
1000 °C	20.5	0.106	1.126	0.252	1.064	1.984

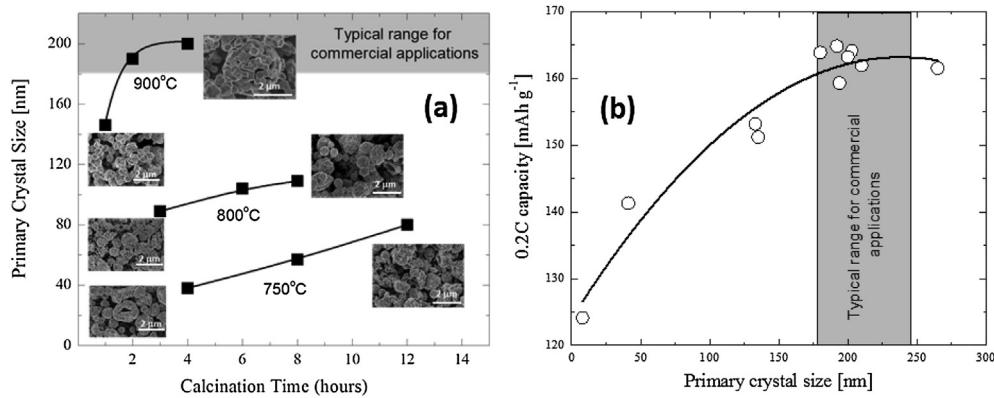


Fig. 3. Relationship between primary crystal size and 0.2 C capacity of NCM prepared by RST.

results in increase of the primary crystal size, which also reduces internal porosity within the spherical agglomerates. Porosity after additional heat treatment at 900 °C for 4 h reduced to only 3% of the porosity of the initial powder after RST process step. However, resulting porosity is still almost five times higher than the total porosity (i.e. pore volume) for NCM powder made by co-precipitation method. It is reasonable to expect that increase in (electrochemically active) surface area combined with internal porosity should result in facilitated reaction kinetics and mass transport (i.e. ionic conductivity). In this mental model, internal pores act as highways for the electrolyte making it accessible to the entire electrochemically active surface area, at rates significantly faster than if Lithium transport was taking place throughout the solid phase (i.e. in large, non-porous particles).

3.2. Electrochemical performance

Electrochemical performance of small particles NCM made by RST processing at 700 °C and post-treated at 900 °C in air for 4 h was compared to co-precipitated large particle NCM of the same composition, i.e. $\text{Li}(\text{Ni}_{0.33}\text{Co}_{0.33}\text{Mn}_{0.33})\text{O}_2$. Both electrodes were optimized with respect to formulation, using Cabot's LiTX200™ carbon conductive additive (CCA). In the case of large particles of co-precipitated NCM, 1 wt.% conductive additive is sufficient and no further rate capability improvement is obtained at higher CCA loading. In the case of a RST made NCM, 3 wt.% CCA is necessary for optimal performance. This is because active materials with small

particle size are less conductive and typically require higher volume (therefore also the mass) fraction of conductive additives to achieve full percolation. CCA and PVDF binder amount were matched in both electrodes, resulting in respectively 98 wt.% NCM:1 wt.% CCA:1 wt.% PVDF and 94 wt.% NCM:3 wt.% CCA:3 wt.% PVDF formulations for large and small particles NCM, respectively. The 0.2 C voltage profile of small particle NCM is similar to NCM obtained by co-precipitation, but the capacity is higher, typically in the range 165–168 mAh g⁻¹ versus 159–160 mAh g⁻¹ for co-precipitation sample. The derivative of voltage profiles are similar, with one pair of reversible peaks bellow 4 V vs. Li^+/Li , indicating that same redox couple ($\text{Ni}^{2+}/\text{Ni}^{4+}$) is active in both cases (Fig. 6).

Discharge curves at different rates for RST made and co-precipitated NCM are shown in Fig. 7. The shape of the curves is similar for both materials, including similar voltage profile in the initial stages of Li intercalation into NCM. This indicates similar resistance to electron flow, and further confirms that optimal loading of conductive additive depends on the morphology of the active material. The differences in polarization curves between two NCM materials made by different process are amplified in later stages of discharge-dominantly under influence of mass transport limitations in the electrode layer. Capacity vs. C-rate plot (Fig. 7(b)) shows that capacity of 137 mAh g⁻¹ at 10 C discharge rate is maintained in electrodes utilizing small particles NCM made by RST process while large particle NCM made by co-precipitation at the same electrode loading is only delivering 97 mAh g⁻¹ (Fig. 7), i.e. >40% improvement is achieved with small particle NCM.

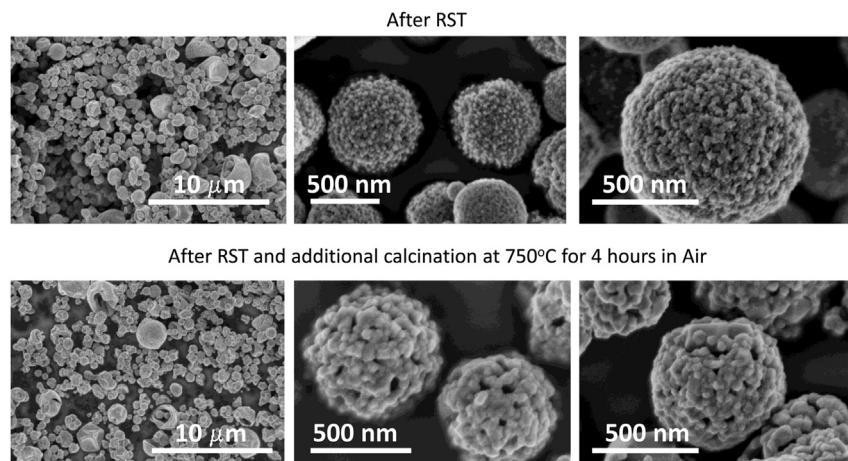


Fig. 4. SEM images at different magnification of material after spray pyrolysis step (700 °C reactor temperature) and after additional calcination at 750 °C for 4 h in air.

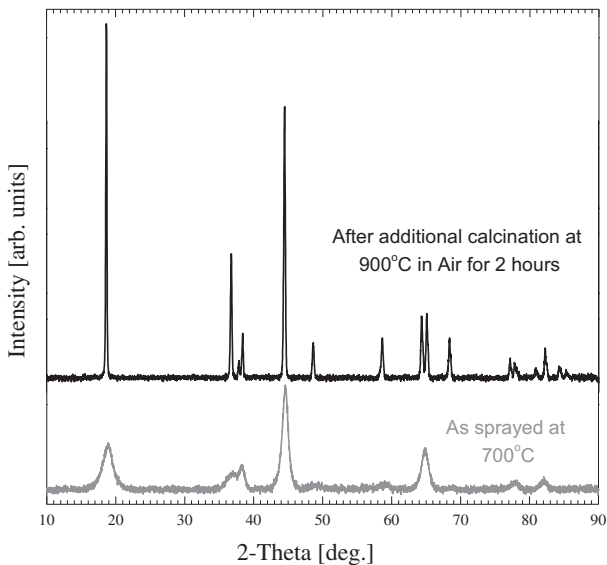


Fig. 5. XRD patterns of $\text{LiCo}_{0.33}\text{Mn}_{0.33}\text{Ni}_{0.33}\text{O}_2$ as sprayed (gray) and after calcination at 900 °C for 2 h in air.

Based on mass normalized Ragone plot, shown in Fig. 8(a), NCM made utilizing RST process demonstrates superior energy density in the entire power range. Volume normalized energy and power density also depends on the electrode density which is in turn the function of the packing properties of the cathode powder. It is well known that smaller particles pack less densely than large particles and reduction in electrode density with RST made material was therefore expected. Under similar calendaring pressure the electrode density of 2.95 g cm^{-3} has been achieved with small RST made NCM particles, compared to 3.52 g cm^{-3} obtained with large co-precipitated NCM. Although further electrode optimization with small NCM made by RST process could reduce this gap further, the difference in density is the result of the fundamental difference in packing of small vs. large particles and cannot be fully eliminated (Fig. 9).

Volume normalized Ragone plot for both NCM particles morphology is shown in Fig. 8(b). The penalty in low electrode density is obvious at low power and now the trend is reversed compared to mass normalized Ragone plot in Fig. 8(a). However, at higher power the gap in energy density is reduced and above certain value it is fully closed. After that point, small and large particle NCM have similar volumetric energy density. When very high discharge power is required, improvement in rate capability of small particles more than compensates for lower packing density

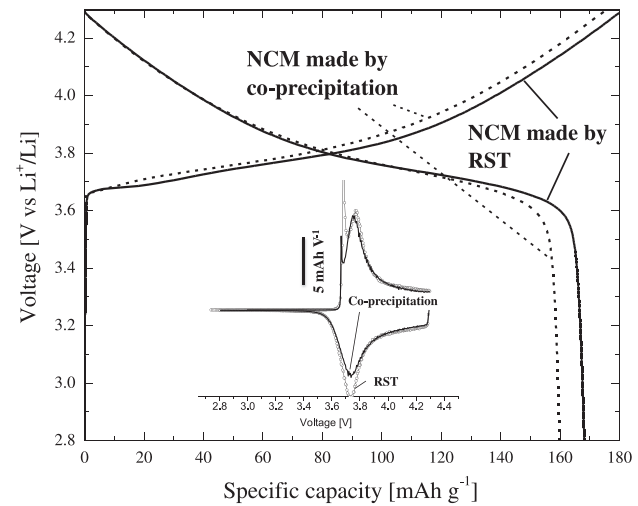


Fig. 6. First 0.2 C charge–discharge voltage profiles and their derivatives (inset) of RST and co-precipitation NCM 111 cathodes.

resulting in volumetric energy and power density on par with large particles of active phase, while still offering almost 50% improvement in gravimetric energy density. Lower electrode density is also indirect evidence for higher electrode porosity in small particles NCM responsible for better capacity retention at high discharge current.

The electrochemical impedance spectra of coin-cells utilizing both large sized NCM made by co-precipitation and small sized NCM made by RST were measured in 1 MHz–1 mHz frequency range with a signal amplitude of 10 mV. In the discharged state, three main features can be observed: first a high frequency

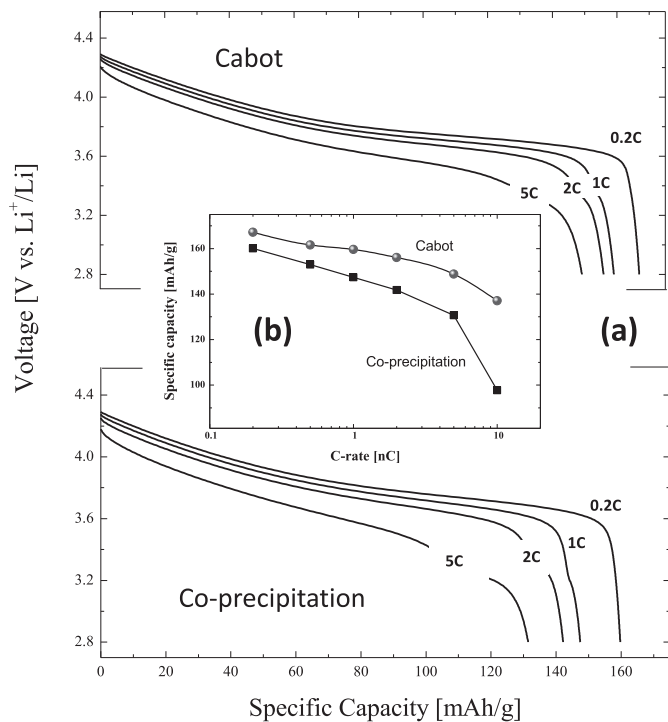


Fig. 7. (a) Discharge curves for RST made and co-precipitated NCM at different discharge rates, (b) specific capacity as a function of discharge rate (C-rate) for the same two materials. Active phase loading was 1.5 mAh cm^{-2} and electrode formulations were optimized using Cabot LiTX200™ carbon black conductive additive.

Table 2
Physical properties of NCM material at different stage of synthesis.

Material	N_2 BET SA ($\text{m}^2 \text{ g}^{-1}$)	Pore volume from single point N_2 BET adsorption ($\text{cm}^3 \text{ g}^{-1}$)	D_{10} (microns)	D_{50} (microns)	D_{90} (microns)
Sprayed at 700 °C	72.7	0.191	0.48	1.24	2.90
Post-treated at 900 °C for 4 h in air	2.05	0.0065	1.14	2.66	4.87
Co-precipitation	0.27	0.0013	5.74	10.93	18.72

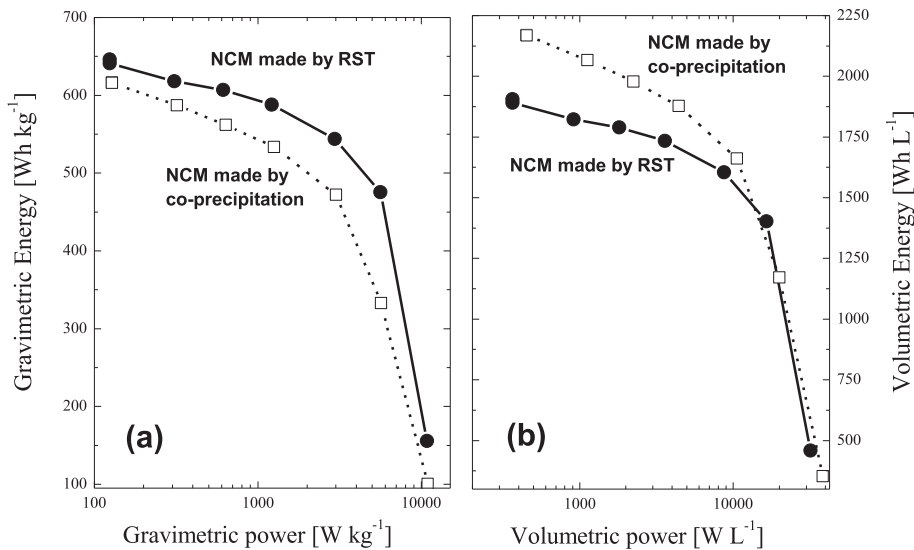


Fig. 8. Gravimetric and volumetric Ragone plots of energy vs. power for RST and co-precipitation NCM 111 cathodes.

intercepts with the real axis, which is indicative of electrolyte resistance (a constant identical for both coin-cells) plus electronic resistance of the electrode, secondly a charge transfer semi-circle, which is indicative of mass transport kinetics through the electrode. And third, at lower frequencies, Warburg diffusion then double-layer capacitance are observed, which reflects the blocking nature of the electrodes in the discharged state. In the case of small particles NCM, higher electronic resistance is observed because smaller particles have higher number of inter-particle connections. However, smaller charge transfer resistance is observed, which we attribute to the faster ionic diffusion of lithium ions inside the smaller porous particles made by RST. This feature results in the higher discharge rate capability observed with the NCM made by this process.

Impact of particle size on cycle-life was investigated under accelerated conditions of 60 °C and 1 C charge–discharge cycling. While small particle NCM showed stable room temperature cycling, the higher surface area NCM was expected to result in higher Mn

dissolution and electrolyte oxidation at elevated temperature, both of which can have detrimental effect on cycle-life. Indeed, this effect was observed at 60 °C, where capacity fade is continuous from the beginning with small particles NCM, while it is delayed for 30 cycles in the case of large particles NCM (Fig. 10). It should be noted here that coin-cells vs. Li metal are not the best systems for this type of tests, and better performance might be possible in full cylindrical or pouch cells using graphite anode. Nevertheless, other approaches such as surface coating or electrolyte additives should also be considered to improve elevated temperature performance of small particles NCM.

In conclusion, small particle NCM prepared on RST platform results in unique morphology characterized by small particle size and significant particle porosity. These materials display promising electrochemical properties in terms of absolute capacity and superior rate capability and are well suited for high power applications. Partial state of charge operation, that could mitigate capacity and performance fade induced by high surface area of active phase

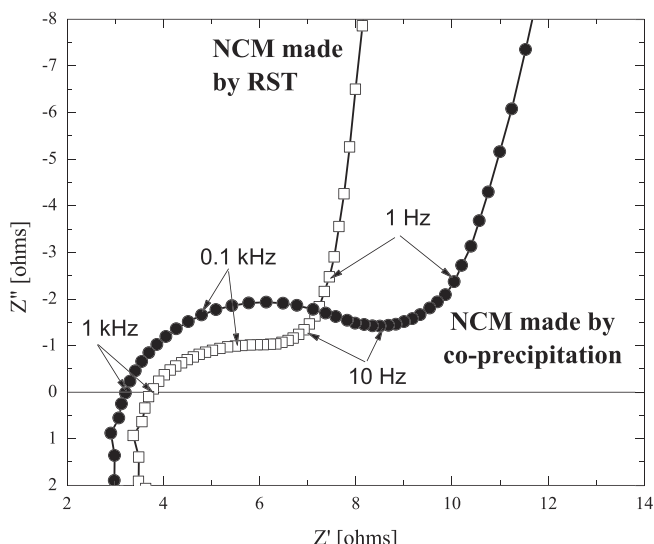


Fig. 9. Electrochemical impedance Nyquist plots of formed and discharged coin-cells with either large or small particle NCM cathodes (coin-cell area = 1.77 cm²).

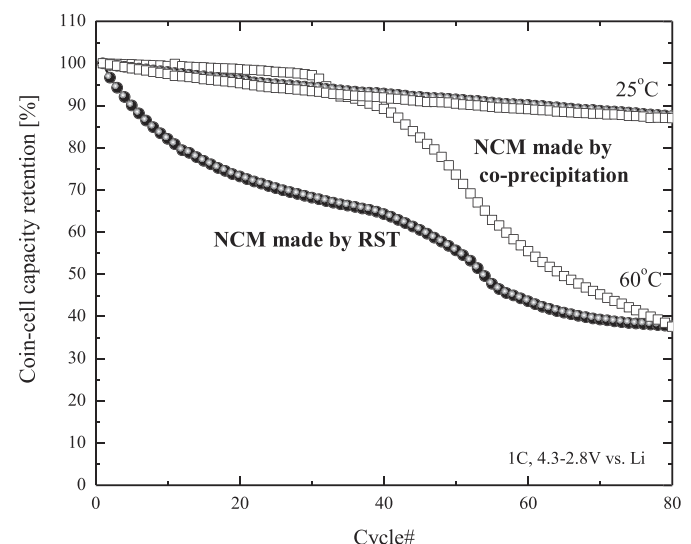


Fig. 10. Capacity vs. cycle life for coin-cells using large co-precipitated or small RST particle cathodes cycled at 1 C and 25 or 60 °C vs. Li metal.

by limiting voltage window and thus slowing the kinetics of electrolyte decomposition, might prove to be particularly suitable for NCM material of such morphology.

In addition, RST process could potentially result in one step production of materials by appropriate design of the reactor temperature and residence time. Even in cases where post-treatment is necessary, the right primary crystal size can be achieved at lower temperatures and shorter treatment time. All this makes RST process promising from the commercial perspective in meeting targets in cost and throughput imposed by Li-Ion battery industry and emerging applications. Although used here to demonstrate benefits of RST in generating unique morphology of NCM particles with superior capacity and rate capability, ultrasonic spray nozzles are not easily scalable for high throughput production. In addition, in-line electrically heated reactor configurations do not lend themselves to easy scale up and large volume production due to the inherent limitations in the heat transfer for externally heated reactors. This prompted us to investigate fluid nozzles as atomization method combined with internally heated reactor configurations with the dual objective of demonstrating particle size control and scalable production, while maintaining the electrochemical performance observed via ultrasonic spray generation based reactive spray conversion process.

3.2.1. RST based on fluid nozzle aerosol generation and internally heated reactor configurations

We have demonstrated benefits of unique morphology of NCM powders made by RST in improving the capacity and rate capability. Unique morphology is described by small particle size and substantial amount of porosity within the spherical agglomerates after spray conversion reaction and optional post-treatment. In case when precursors are in the solution phase, RST relies on liquid-to-solid conversion where liquid droplets (containing precursor species) are introduced into the thermal reactor where they undergo physical and chemical transformations, schematically shown in Fig. 1. Each droplet becomes a particle during spray pyrolysis and direct correlation can be established between the droplet and the final particle size of the powdered material. Therefore, generation of powders with small particle size require generation of small droplets. In previous examples, small droplet and thus particle size was achieved using submerged ultrasonic atomizer operating at 1.65 MHz. The ultrasonic atomizers are attractive for materials processing by spray pyrolysis because of their low spray velocity, relatively low amount of carrier gas required, simplicity, high concentration of droplets, and the most importantly the small droplet size produced. This makes ultrasonic generators the atomizers of choice in most of the small scale and laboratory spray pyrolysis systems. However, the major disadvantage of this type of atomizer is the low liquid delivery rate, and thus low powder production rate. As such, ultrasonic atomizers are inherently difficult to scale up to production throughput required for sufficiently optimized economy of scale and processing cost required by Li-Ion battery industry. On the other hand, pressure and two-fluid

atomizers are capable of high liquid delivery rates, thus resulting in high powder generation rates, but typically generation of high concentration of small droplets with this atomization processes is much more difficult. Two-fluid atomizers use the kinetic energy of gas for atomization process. The atomization is created due to high frictional shearing forces between the liquid surface and the gas having high velocity. Compressed air is the most often used as atomizing gas, but other gasses are also used.

Having requirements for production throughput and conversion cost required by Li-ion battery industry in mind, we have explored proprietary two-fluid (air-assist) nozzle configurations capable of generating droplets in a wide size range. These fluid nozzles were paired with internally heated reactor configurations. Final particle size of powders produced under different fluid nozzle conditions ranged from size comparable to ultrasonic atomization process, to particles significantly larger than those obtained by typical co-precipitation method. Table 3 lists physical properties of powders made with fluid nozzle at three different conditions, and compare them to powders made by RST process using ultrasonic droplet generation as well as NCM made by co-precipitation method. Operation of fluid nozzle under condition 1 generated powder with very similar properties as the one generated using ultrasonic atomization unit, while operation of fluid nozzle under conditions 2 generated larger particles. Finally, operation of fluid nozzle under conditions 3 generated powder with much larger particles and particle size distribution comparable to NCM typically made by co-precipitation method. Morphology of powders, made by fluid nozzle atomization unit paired with internally heated reactor configuration, resembled closely NCM material made by RST process using ultrasonic droplet generation and in-line electrical heat source, i.e. all powders retained substantial amount of porosity within the spherical agglomerates, as shown in Table 3 and Fig. 11. All RST made samples listed in Table 3 were thermally post-treated at 900 °C for 4 h after the RST conversion step. Surface area of calcined samples made using different atomization processes and conditions ranged from 1.29 to 2.5 m² g⁻¹.

While in previous examples electrode formulations have been optimized in terms of the amount of conductive additive and binder, here such optimization was not performed for initial screening. In order to understand the impact of cathode morphology on lithium transport, both through the solid and liquid phase, and to enable meaningful comparison between different systems at higher discharge rates, we have deliberately overloaded the electrode formulation with conductive carbon to ensure performance is not limited by electronic conductivity. We have used "Argonne National Laboratory" formulation calling for 4 wt.% conductive carbon black, 4 wt.% of graphite and 8 wt.% of the PVDF [25]. High loading of carbon black insures enough of the conductive pathways for electrons, while graphite, in addition to providing electrical conductivity, also act to control the pore size within the electrode and therefore mitigate negative impact of high loading of carbon black and binder in reducing the pore size. This effectively resulted in the reduced loading of the active phase to 84% by

Table 3

Physical properties of NCM powders made with different processes and atomization methods.

NCM made by:	N ₂ BET SA (m ² g ⁻¹)	Pore volume from single point N ₂ BET adsorption (cm ³ g ⁻¹)	D _{mean} volume (microns)	D ₁₀ (microns)	D ₅₀ (microns)	D ₉₀ (microns)
RST; ultrasonic atomization	2.05	0.0054	2.9	1.14	2.66	4.87
RST, fluid nozzle, conditions 1	1.53	0.0040	3.9	1.8	3.2	6.5
RST, fluid nozzle, conditions 2	1.29	0.0033	7.4	2.4	5.9	14.0
RST; fluid nozzle, conditions 3	2.5	0.0073	16.7	7.6	14.7	27.21
Co-precipitation	0.27	1.2	11.8	5.7	10.9	18.7

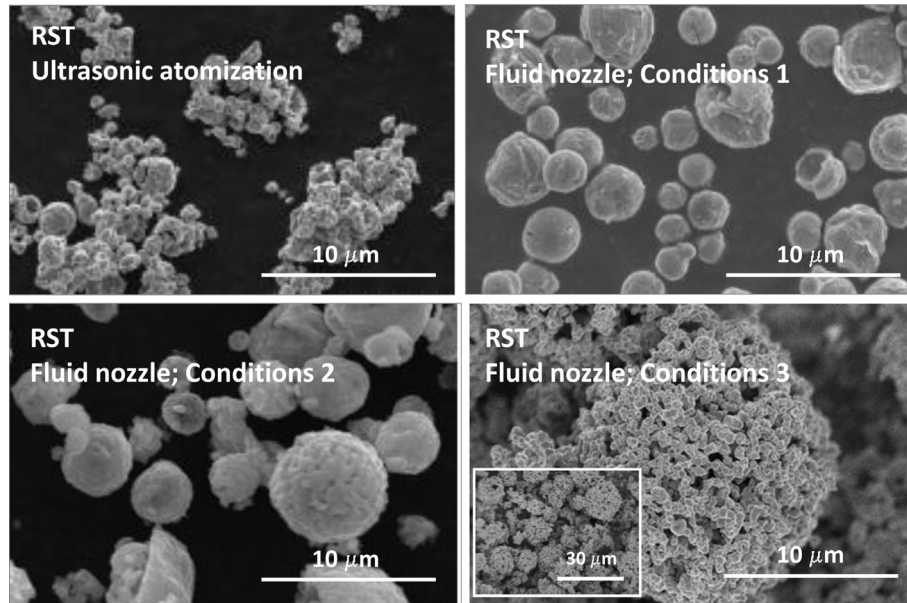


Fig. 11. SEM images of RST-made NCM particles prepared by ultrasonic atomization, and fluid nozzle at three different operating conditions.

weight. Electrochemical performance can therefore be further optimized and overall performance improved, but we believe that these conditions result in meaningful initial comparison between powders of different morphology. However, due to the lack of the electrode optimization Ragone plots, especially volume normalized, have limited value and were not considered with these samples.

Polarization curves during discharge at different rates up to 5 C are shown in Fig. 12. Benefit of small particles, made by RST and using ultrasonic aerosol generation, in rate performance compared to large NCM particles made by co-precipitation is demonstrated again, although the absolute numbers are lower than of fully optimized electrodes. Further electrode optimization could result in improvement in absolute performance, but the trends are expected to remain unaffected.

Capacity utilization at low rate correlates with the size of the secondary agglomerates made of aggregated primary crystals, as shown in Figs. 12 and 13. Smaller particle size results in increased capacity utilization at both low and high discharge rates. NCM powder made by RST using fluid nozzle and conditions 1 performs similarly as the NCM powder made by RST using ultrasonic aerosol generator. This result is not surprising, considering similar particle size and particle size distribution for both, but it is significant since it demonstrates path to large scale and volume production of cathode materials with unique morphology. The material produced using fluid nozzle generation under conditions 1 has slightly larger particles and lower electrochemical surface area, resulting also in lower internal particle porosity (Table 3). Consequently high rate performance is lower compared to NCM powder made by spray pyrolysis using ultrasonic droplet generation. This material was made without systematic optimization of fluid nozzle and reactor operating conditions. Subsequently, we believe that electrochemical performance of material made in such way can be further improved and potentially fully match the performance of NCM material made after ultrasonic droplet generation in smaller electrically heated reactor.

Another example of special interest is powder made by RST process, using fluid nozzle under conditions 3. As can be seen from Table 3 and Fig. 11, particle size and particle size distribution is

shifted to larger size compared to NCM made by co-precipitation method. Still, material made by RST process have different morphology, the most important being internal porosity within the spherical agglomerates. This sample is therefore best suited to explore relative importance of internal porosity and the particle

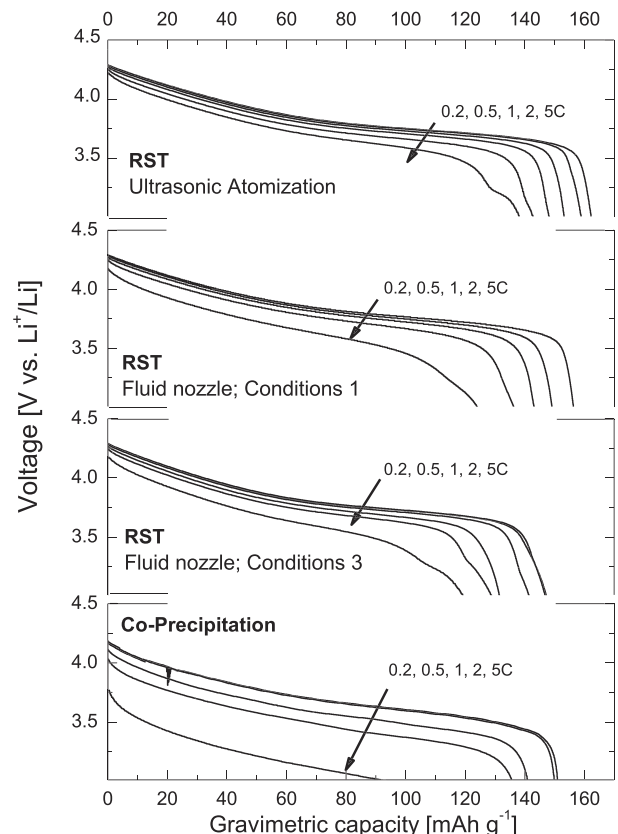


Fig. 12. Specific capacity vs. voltage at 0.2, 0.5, 1, 2, 5 C discharge rates for NCM cathodes as function of preparation method.

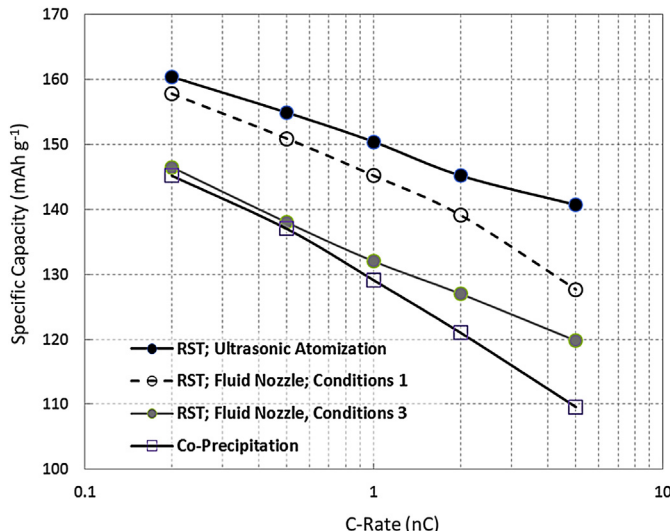


Fig. 13. C-rate performance of NCM cathodes obtained by various preparation methods.

size in mass transport at high discharge rates. Based on Figs. 12 and 13, initial capacity utilization at low discharge rates is similar to the NCM made by co-precipitation method. At high discharge rate benefit of internal porosity is obvious and RST made NCM powder outperforms NCM made by co-precipitation. At very high discharge rates, the performance is positively impacted by high electrochemical surface area and existence of internal pore network responsible for delivering Li ions to the surface of the active phase. Combination of these two features of the powder was able to compensate for the larger size of spherical agglomerates. Control over the size of spherical agglomerates and their size distribution, while maintaining unique morphology, opens possibility to further optimize the packing density of the powders made by RST.

4. Conclusions

The NCM powders with controlled particle size, composition and morphology were prepared by reactive spray technology. Only mild post-treatment at 800–900 °C for 2–4 h was adequate to achieve excellent electrochemical performance. For small particle NCM (1–2 μm), the initial discharge capacity was 167 mAh g⁻¹ at the discharge rate of 0.2 C, and material retained 82% of that capacity when going from 0.2 C to 10 C rate. For comparison, electrodes made of 10 μm commercial NCM particles, at the same loading and optimized with LiTX200 carbon black conductive additive, delivered 160 mAh g⁻¹ at 0.2 C, and retained only 61% of that capacity at 10 C rate.

Larger particle NCM have similar initial capacity but exhibit more pronounced capacity decrease at higher C rates. Better performance of small particles NCM originates from improved mass transport in the electrode, and is the result of combined effect of two factors. First factor is at the particle level – solid state diffusion length of lithium is reduced because of the reduced particle size. Second factor is on the electrode level – ion transport is facilitated by higher porosity within the active particles, which is evidenced by their lower packing density. However, lower packing density reduces volumetric energy density. In addition, smaller particles size results in larger capacity decay during high temperature cycling. Effort is currently underway to resolve some of those issues, and results will be reported in the future. The RST appears to be a promising technique for industrial-scale production of the cathode materials for lithium ion batteries.

Acknowledgments

Authors are thankful to Joe Slanga and Cabot Analytical Group for performing analytical work.

References

- [1] M. Armand, J.-M. Tarascon, *Nature* 414 (2001) 359–367.
- [2] M. Armand, J.-M. Tarascon, *Nature* 451 (2008) 652–657.
- [3] T. Ohzuku, Y. Makimura, *Chem. Lett.* 30 (2001) 642.
- [4] I. Belharouak, Y.K. Sun, J. Liu, K. Amine, *J. Power Sources* 123 (2003) 247.
- [5] M.H. Lee, Y.J. Kang, S.T. Myung, Y.K. Sun, *Electrochim. Acta* 50 (2004) 939.
- [6] J. Choi, A. Manthiram, *Electrochim. Solid State Lett.* 7 (2004) A365.
- [7] Y.Y. Huang, J.T. Chen, J.F. Ni, H.H. Zhou, X.X. Zhang, *J. Power Sources* 188 (2009) 538.
- [8] M.M. Thackeray, S.H. Kang, C.S. Johnson, J.T. Vaughey, S.A. Hackney, *Electrochim. Commun.* 8 (2006) 1531.
- [9] F. Zhou, X.M. Zhao, J.R. Dahn, *J. Electrochim. Soc.* 156 (2009) A343.
- [10] X.Y. Zhang, W.J. Jiang, A. Mauger, Q.F. Gendron, C.M. Julien, *J. Power Sources* 195 (2010) 1292.
- [11] B.J. Hwang, Y.W. Tsai, D. Carlier, G. Ceder, *Chem. Mater.* 15 (2003) 3676.
- [12] S.H. Park, C.S. Yoon, S.G. Kang, H.S. Kim, S.I. Moon, Y.K. Sun, *Electrochim. Acta* 49 (2004) 557.
- [13] D.C. Li, T. Muta, L.Q. Zhang, M. Yoshio, H. Noguchi, *J. Power Sources* 132 (2004) 150.
- [14] S.H. Ju, Y.C. Kang, *Ceram. Int.* 35 (2009) 1633–1639.
- [15] H.S. Kang, Y.C. Kang, H.D. Park, Y.G. Shul, *Mater. Lett.* 57 (2003) 1288–1294.
- [16] M. Eslamian, N. Ashgriz, *Powder Technol.* 167 (2006) 149–159.
- [17] A. Bayu, D. Nandiyanto, K. Okuyama, *Adv. Powder Technol.* 22 (2011) 1–19.
- [18] S.-H. Park, S.W. Oh, Y.-K. Sun, *J. Power Sources* 146 (2005) 622–625.
- [19] H.M. Wu, J.P. Tu, X.T. Chen, Y.F. Yuan, Y. Li, X.B. Zhao, G.S. Cao, *J. Power Sources* 159 (2006) 291–294.
- [20] Y. Li, C. Wan, Y. Wu, C. Jiang, Y. Zhu, *J. Power Sources* 85 (2000) 294–298.
- [21] X. Zhang, H. Zheng, V. Battaglia, R.L. Axelbaum, *J. Power Sources* 196 (2011) 3640–3645.
- [22] N.A. Hamid, S. Wennig, S. Hardt, A. Heinzel, C. Schulz, H. Wiggers, *J. Power Sources* 216 (2012) 76–83.
- [23] S.H. Ju, Y.C. Kang, *J. Alloys Compd.* 469 (2009) 304–309.
- [24] M.J. Hampden-Smith, T.T. Kodas, J. Caruso, Q.H. Powell, US Patent 6,770,226 B2, 2004.
- [25] C.S. Johnson, J.S. Kim, A.J. Kropf, A.J. Kahaian, J.T. Vaughey, L. Fransson, K. Edström, M.M. Thackeray, *Chem. Mater.* 15 (2003) 2313.